Extracting Free Energies of Salt Ion Binding to Polyelectrolytes by Molecular Dynamics Simulations

Wen-de Tian, 1,2 Mohsen Ghasemi, 2 and Ronald G. Larson 2*

Abstract

We use all-atom molecular dynamics (MD) simulations to extract ΔG_{AS}^{eff} , the free energy of binding of potassium salt ions K^+ to the partially charged polyelectrolyte poly(acrylic acid), or PAA. Upon increase of the charge fraction of PAA, the chains adopt more extended conformations, and simultaneously, potassium ions bind more strongly (i.e., with more negative ΔG_{AS}^{eff}) to the highly charged chains to relieve electrostatic repulsions between charged monomers along the chains. We compare the simulation results with the predictions of a model that describes potassium binding to PAA chains as a reversible reaction whose binding free energy (ΔG_{AS}^{eff}) is adjusted from its *intrinsic* value (ΔG_{AS}) by electrostatic correlations, captured by a random phase approximation (RPA). The bare or intrinsic binding free energy ΔG_{AS} , which is an input in the model, depends on the binding species and is obtained from the radial distribution function of K^+ around the charged monomer of a singly-charged PAA chain in dilute solutions. We find that the model yields semi-quantitative predictions for ΔG_{AS}^{eff} and the degree of potassium binding to PAA chains, α_{AS} , as a function of PAA charge fraction, without using fitting parameters.

1. Introduction

Polyelectrolytes (PEs) are ionized or ionizable polymers that enable a diverse set of biological and technological applications due to their rich physiochemical properties. Examples include the formation of membraneless organelles, ¹⁻³ chromosome packaging, ⁴ cellular organization, ⁵ virus self-assembly, ⁶ as well as DNA transfection into cells, ⁷ stabilization of vaccines, ⁸ delivery of therapeutics into the body, ^{9,10} and self-assembly of materials with various morphologies, ¹¹ including thin films. ¹²⁻¹⁵ Many of these and other applications involve formation of polyelectrolyte complexes (PECs) from the association of oppositely charged polyelectrolytes. Given their importance and ubiquity, PEs have attracted extensive attention, but a satisfactory theoretical description of their equilibrium behavior in solution has remained elusive. This arises from the correlated nature of electrostatic interactions, which are coupled to chain configurations, and also from local binding between charge groups that is sensitive to their chemical specificity.

In this study, we seek to develop a computational method for predicting key parameters needed for comprehensive accounting of the thermodynamics of polyelectrolyte solutions, focusing on aqueous solutions

Center for Soft Condensed Matter Physics and Interdisciplinary Research, Soochow University, Suzhou 215006, China
Department of Chemical Engineering, University of Michigan, Ann Arbor, Michigan 48109

of polyanions and their counterions. A simple theory to treat the electrostatic interactions in solutions containing charged species is the Debye-Hückel (DH) theory, ¹⁶ which predicts the distribution of (small) ions near a test ion. The DH theory usually works best for electrolyte solutions at low ionic strengths, and, although it does not capture the monomer connectivity of polyelectrolyte chains, ^{17,18} it has been applied to polyelectrolyte solutions by Voorn and Overbeek. ¹⁹ To remedy the deficiencies of the DH theory, more recent approaches, such as field theoretic simulations (FTS)^{20–22} and the random phase approximation (RPA), ²³ have included the electrostatic correlations due to chain connectivity and form factor of PE chains. In the RPA theories, however, the polyelectrolyte structure, which reflects the PE chain connectivity, is fixed, and does not respond to changes in the solution condition, such as the concentrations of species. ^{17,18} Recently, the assumption of fixed PE structure was relaxed using a variational approach to the electrostatic free energy of polyelectrolytes. ¹⁷

Inherent in the aforementioned theories is that counterions (or, salt ions) and PE monomers are modeled as generic spheres or point charges interacting through long-range electrostatics at all length scales, despite the fact that ion specificity (such as the hydration level of the ions and monomers) impacts the interaction of salt ions with oppositely charged monomers at short distances.^{24–26} For instance, the response to added salt of the swelling of PECs²⁷ and the viscosity²⁸ of single-polyelectrolyte solutions show that the more "hydrophobic" salt anions, with fewer waters of hydration, tend to localize (or bind) along polyelectrolytes more strongly than do highly hydrated ones. In addition, the activity of counterions in the presence of polyelectrolytes deviates strongly from that of simple electrolyte solutions at the same ionic strength due to localization of counterions in the vicinity of the polymer chains.²⁹ In fact, these ion-specific effects were manifested through the experimental observations of Hofmeister on protein stability over 100 years ago.³⁰

Manning, who was among the first to model the binding of ions to polyelectrolytes, ^{31–33} suggested that when the Coulomb energy between two (neighboring) charged monomers along the PE is higher than the thermal energy of a (free) ion in the solution, an ion from the solution condenses onto the PE. This prediction, while qualitatively correct, ignores the aforementioned specificity in the localization of ions along polyelectrolytes, motivating multiple efforts to incorporate ion-specific effects into the treatment of ion-PE interactions. ^{34,35,44–46,36–43} A recent example is that of Sammalkorpi and co-workers, who added an additional ion-PE-specific interaction potential to the electrostatic potential in their Poisson-Boltzmann model. ³⁴ The Sing group, on the other hand, used a "transfer matrix" (TM) to include the effects of neighboring monomer correlations along the chain in the probability of binding of oppositely charged groups, where the strength of this local correlation was obtained from molecular simulations. ^{37–41} In the theory of Muthukumar and coworkers, the degree of salt ion binding to a PE was obtained self-consistently; however, the electrostatic correlations were treated using the DH theory. ^{35,36} Ermoshkin and Olvera de la Cruz, on the other hand, used a random phase approximation (RPA) to determine the contribution of electrostatic correlations to the equilibrium constant of ion binding to polyelectrolytes. ⁴²

More recently, similar to Ermoshkin and Olvera de la Cruz, Friedowitz, Salehi, Larson and co-workers^{43–45} developed a theory that treats the electrostatic correlations using a RPA and describes ion-PE binding as a reaction with a self-consistently derived equilibrium constant. Within this theory, the binding of ions to polyelectrolytes is driven by an intrinsic free energy of binding, ΔG , and also by a contribution from

electrostatic correlations between charged groups, μ^{corr} , obtained from the RPA.^{43,46} The latter contribution is non-ion-specific although it does depend on the structure of polyelectrolyte chain and fluctuation of charges, within the RPA theory, as discussed later.^{43,46} The intrinsic binding strength or ΔG , on the other hand, is defined as the standard-state free energy of binding of a salt ion to a monomer (of a polyelectrolyte) in infinite dilution.⁴⁴ ΔG therefore accounts for changes in water structure upon binding, and enhanced electrostatics as a result of the low dielectric constant near PE monomers. While this ΔG is ion-specific, it has to date been taken as an adjustable constant for each salt ion-PE monomer pair. To make the theory predictive, a means of obtaining the relevant ΔG values a priori is needed for specific ions and polyelectrolytes.

In this work, to estimate a priori the value of ΔG needed for the theories described above, we use molecular simulations, here focusing on the binding of potassium ions onto charged poly(acrylic acid), or PAA, chosen because of its relatively simple chemical repeat unit. Since PAA is a weak polyelectrolyte whose charge level is set by pH, and we use standard molecular dynamics (MD) simulations without reactive forcefields, we impose a priori an ionization state onto PAA oligomers (whose charge fraction is related to the experimental pH), for which we then compute the degree of salt ion binding. We choose both short, 5-monomer, PAA chains, each with only one charged and four neutral monomers, as well as longer PAA chains with varying fractions of ionized monomers. At very low ionization fractions in the MD simulations, potassium ions bind only weakly along chains, but increasing the charge fraction leads to strong localization (i.e., binding), in agreement with the literature. ⁴⁷ We incorporate these results into the RPA theory of Friedowitz et al. for each ionization fraction, using either a polyelectrolyte form factor obtained directly from the MD simulations or a pre-determined form factor such as that of a rod or a Gaussian coil. 43 We find that in the limit of highly ionized PAA chains, the aforementioned strong localization of potassium ions relieves the repulsions between charged monomers, described through μ^{corr} . In this limit and using either the rodlike chain or the chain configuration obtained from MD simulations, our model yields quantitatively accurate predictions for the fraction of bound potassium ions on PAA, without using any fitting parameter.

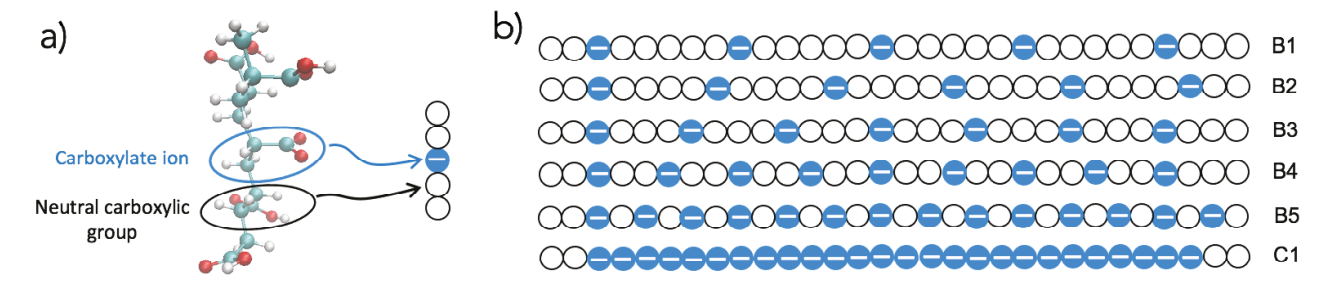
This work is organized as follows: A concise description of the technical details of the MD simulations along with the aforementioned theory are presented in Section 2. We discuss the simulation and theoretical results in Section 3, and draw conclusions in Section 4.

2. Methods and Theory

2.1. Simulation Systems

The simulation systems investigated in this study are listed in Table 1. Each contains PAA chain(s), potassium ions, and water molecules in a cubic box of length *L*. Systems A1 through A5 contain different numbers of short PAA chains, each with five monomers, with the central one charged. Systems B1 through B5 each contain a single, longer, 30-monomer PAA chain with varying charge fraction (see Figure 1). Systems C1 through C3 include nearly fully charged PAA chains with different degrees of polymerization. Note that, in this work we keep neutral the final two monomers at each end of the chain (four monomers in all) to reduce the end chain

effects, and the charge fraction γ of the chain is then based on the remaining $N_{\text{chain}} - 4$ monomers. (For instance, the charge fraction of system C1 is 1.)



Singly-charged, 5 monomer PAA chain

30 monomer PAA chains with varying charge fractions

Figure 1. (a) Singly-charged PAA chain with 5 monomers, in which the central monomer carries a negative charge due to the carboxylate ion. (b) 30-monomer PAA chains with different number of charged monomers corresponding to systems B1 through B5 and C1 in Table 1. Open circles represent neutral monomers, and blue ones are those carrying the charged carboxylate ions.

Table 1. Details of simulation systems: $N_{\rm chain}$ denotes the number of PAA chains in the simulation box, $N_{\rm P}$ is the degree of polymerization (or number of monomers per chain), $N_{\rm cP}$ the number of charged monomers per chain, $\gamma = N_{\rm cP}/(N_{\rm P}-4)$) the "charge fraction" of each chain as defined in the text, $N_{\rm W}$ the number of water molecules, and L the size of the cubic simulation box. For chains of fixed length and varying charge fraction (i.e., systems B1 through B5), the charged monomers were equally spaced along the chain (see Figure 1). In this work, the PAA chains are of isotactic stereochemistry.

System	$N_{\rm chain}$	$N_{ m P}$	$N_{\rm cP}$	γ	$N_{ m W}$	L (nm)
A1	5	5	1	N.A.	31670	9.84
A2	10	5	1	N.A.	31670	9.84
A3	20	5	1	N.A.	31670	9.86
A4	30	5	1	N.A.	31670	9.86
B1	1	30	5	0.19	23610	8.92
B2	1	30	6	0.23	23596	8.92
В3	1	30	7	0.27	23602	8.91
B4	1	30	9	0.35	23589	8.91
В5	1	30	14	0.54	32442	9.91
C1	1	30	26	1	32398	9.90
C2	1	41	37	1	32597	9.93
C3	1	56	52	1	56337	11.91

2.2 Simulation Details

All MD simulations were performed with GROMACS (version 2019.3), 48 in which the GAFF force field 49 was used to evaluate interactions between PAA chains and K⁺. The partial charges on PAA were obtained from the recent work of Mintis et al. 50 The water molecules (SPC/E model), counterions, and PAA chains were randomly placed in the simulation box. Then, energy minimization was applied by the steepest descent algorithm with a convergence criterion that the maximum force on any atom not exceed 800 kJ mol⁻¹ nm⁻¹. Subsequently, a short 60 ps simulation under isothermal—isochoric conditions (NVT ensemble) at temperature T = 298.15 K was carried out using the leap-frog algorithm to integrate Newton's equations of motion with an

integration time step of 1.5 fs. Production runs with a time step of 2 fs were performed in the isothermal-isobaric conditions (NPT ensemble) at T = 298.15 K and pressure P = 1.0 atm, kept fixed using the Nose-Hoover thermostat⁵¹ and the Parrinello-Rahman barostat,⁵² respectively. The total simulation time for each case was 100 ns and the trajectories and energies were stored every 5 ps. The last 60 ns were used to calculate the structural quantities.

The simulation box was cubic with periodic boundary conditions in all the three directions. The van der Waals interactions were accounted for by Lennard-Jones potentials truncated at $r_c = 1.2$ nm. The electrostatic interactions were calculated using the particle mesh Ewald (PME) technique⁵³ with a Fourier spacing of 0.12 nm. All bonds in the polymer chain were constrained using the LINCS algorithm.⁵⁴

2.3 Calculation of Static Properties from MD simulations

The configuration of the PAA chain with different degrees of deprotonation in the solution is quantified by its mean-square end-to-end distance:

$$\langle R_e^2 \rangle = \langle (\mathbf{r}_{N_{\rm P}} - \mathbf{r}_1)^2 \rangle \tag{1}$$

where r_1 and $r_{N_{\rm P}}$ denote the positions of the first and last monomers of the chain, respectively.

The distribution of counterions around a charged PAA monomer are described by the radial distribution function (RDF), g(r),

$$g(r) = \frac{n(r)}{\bar{\rho}V(r)} \tag{2}$$

where n(r) is the average number of ions in a spherical shell of thickness Δr and volume $V(r) \approx 4\pi r^2 \Delta r$ at the radial distance, r, from the center of mass of each charged monomer, and $\bar{\rho}$ is the average number density of surrounding ions in a sphere of radius half the box dimension, or, almost equivalently, the overall number density of ions in the box.

2.4 Extracting binding fraction and effective binding free energy from MD simulations[LR1]

Using an equal molarity C_0 of potassium ions and of charged PAA monomers in the simulation box, the salt ions reversibly bind to the charged groups of the PAA chain(s); i.e.,

$$MA^- + K^+ \stackrel{\Delta G_{AS}^{eff}}{\Longrightarrow} MA \bullet K$$
 (3)

Here MA⁻ denotes negatively charged monomers on the PAA chain that are *free* or unbound by a salt ion, K⁺ denotes *free* potassium ions, and MA•K is a charged monomer paired with a potassium ion. In reaction (3), ΔG_{AS}^{eff} denotes the effective free energy of salt (i.e., potassium) binding to a charged group of PAA. Species and charge conservation gives,

$$[K^+] + [MA \bullet K] = C_0 \tag{4}$$

$$[\mathsf{M}\mathsf{A}^-] + [\mathsf{M}\mathsf{A}\bullet\mathsf{K}] = C_0 \tag{5}$$

[x] represents the molar concentration of x. (Clearly, due to the electroneutrality condition, we have $[K^+] = [MA^-]$.) We will discuss how we distinguish between free and bound potassium ions in the Results section. One can write the equilibrium constant of the reaction (3), \mathcal{K}_0 , as,

$$\mathcal{K}_0 = \frac{[\mathsf{MA} \bullet \mathsf{K}]}{[\mathsf{MA}^-][\mathsf{K}^+]} \tag{6}$$

However, this equilibrium constant has units (L/mol). To make it dimensionless and normalized, we multiply it by the concentration of water at standard conditions, [water] $_0 = 55.5 \text{ mol/L},^{44} \text{ leading to},$

$$\mathcal{K}_{MD} = \frac{[MA \bullet K] [water]_0}{[MA^-] [K^+]}$$
(7A)

which can be written as,

$$\mathcal{K}_{MD} = \frac{[MA \cdot K]}{[MA^{-}]M_{S}^{f}} \tag{7B}$$

$$= \frac{\alpha_{\rm AS}}{(1 - \alpha_{\rm AS}) \,\mathrm{M_S^f}} \tag{7C}$$

Here $\alpha_{AS} = \frac{[MA \cdot K]}{c_0}$ denotes the salt binding fraction, and we have taken $M_S^f = \frac{[K^+]}{[water]_0}$ to be the mole ratio of free salt to water. Given the incompressibility of polyelectrolyte solutions and high-water content of the simulation box (see Table 1), we will relate M_S^f to the volume fraction of free salt ϕ_S^f later. Equation (7C) also resembles closely the equilibrium constant in Langmuir adsorption, with the difference that α_{AS} is replaced by surface coverage and M_S^f is replaced by the partial pressure of a free adsorbate. As will be introduced shortly, Equation (7C) is, however, a special case of the equilibrium constant of salt binding to PE from our theory, where the ion size is set equal to the size of a water molecule. Upon finding concentrations of free and bound potassium from MD simulations, we can use one of Equations (7) to find calculate \mathcal{K}_{MD} and then obtain the effective free energy of binding of potassium ions to PAA using $\Delta G_{AS}^{eff} = -\ln \mathcal{K}_{MD}$ (assuming equality of the sizes of ion and water molecules).

2.5 Theory

Our theory treats ion binding to PEs as a reversible reaction, whose free energy is adjusted by electrostatic correlations. Minimization of free energy in our theory (see refs ^{43,44,55}) with respect to the degree of ion binding (to PEs) leads to the following equilibrium constant,

$$\mathcal{K}_{\text{theory}} = \frac{\alpha_{\text{AS}}}{(1 - \alpha_{\text{AS}}) \,\phi_{\text{S}}^{\text{f}}} = \exp\left[-\Delta G_{\text{AS}} - \mu_{\text{AS}}^{\text{corr}} + 1\right] \tag{8A}$$

$$= \exp\left[-\Delta G_{\rm AS}^{\rm eff}\right] \tag{8B}$$

with $\Delta G_{AS}^{eff} = \Delta G_{AS} + \mu_{AS}^{corr} - 1$ and,

$$\mu_{\rm AS}^{\rm corr} = -\frac{1}{\pi} \frac{l_{\rm B}}{\ell} \int_0^\infty \left(\hat{\Gamma}^2(q, a_{\rm S}) + 2N_{\rm cP} \sigma_{\rm A} \hat{\Gamma}^2(q, a_{\rm A}) P(q) \right) / \left(1 + \frac{\tilde{k}^2(q)}{q^2} \right) dq \tag{9}$$

The volume fraction of free ion ϕ_S^f is related to its mole ratio M_S^f through $\phi_S^f = \omega_S M_S^f$, where ω_S is the normalized size of the ion defined as $\omega_S = \frac{v_S}{v_W}$ with v_i the molecular volume of species i, with i = S for salt ion, i = W for water. Here ΔG_{AS} is the intrinsic binding free energy between the polyanion monomer and the K^+ salt ion, which is an input into the theory and will be measured in MD simulations in this work. ΔG_{AS} captures all specific effects in ion-monomer binding in infinite dilution. The contribution of electrostatic interactions to ion binding is given by μ_{AS}^{corr} which depends on the chain form factor P(q) within the random phase approximation (RPA). The form factor in the RPA is fixed and should not in principle be perturbed by the electrostatic interactions. We will use either a pre-defined chain form factor (such as rod or Gaussian coil) or one obtained from the MD simulations themselves. However, although the chain configurations from the MD simulations are obviously affected by electrostatic interactions, feeding such configurations into the RPA could improve the deficiency of the RPA due to its inability to capture chain configuration adjustment to solution conditions and electrostatic interactions. The form factor from MD simulations itself can be calculated in two ways, either using the charged monomer-charged monomer RDF, $g_{CP-CP}(r)$, $f_{CP-CP}(r)$.

$$P(q) = \frac{1}{N_{cP}} \left(1 + 4\pi \bar{\rho} \int_0^{r_{\text{max}}} r^2 \left(g_{cP-cP}(r) - 1 \right) \frac{\sin(qr/\ell)}{qr/\ell} dr \right)$$
 (10A)

or using the formula, 21,57

$$P(q) = \frac{1}{N_{cP}} < \left[\sum_{i=1}^{N_{cP}} \sin(q \ r_i / \ell) \right]^2 > + \frac{1}{N_{cP}} < \left[\sum_{i=1}^{N_{cP}} \cos(q \ r_i / \ell) \right]^2 >$$
 (10B)

In the above, q is the wavenumber and \mathbf{q} the wave vector $\mathbf{q} = (q_x, q_y, q_z)$ in Fourier space, which are normalized by the reference length $\ell = v_W^{1/y}$. N_{cP} is the number of charged monomers per chain, given in Table 1 for different systems. In Equation (10A), r_{ma} is half the box size (L), and in Equation (10B) \mathbf{r}_i denotes the position of the ith charged monomer of the PE chain.

In the expression for μ_{AS}^{corr} (Equation 9),

$$\tilde{k}^2 = 4\pi \frac{l_{\rm B}}{\ell} \left(\frac{\phi_{\rm S}^{\rm f}}{\omega_{\rm S}} \hat{\Gamma}^2(q, a_{\rm S}) + \frac{\phi_{\rm A}}{\omega_{\rm A}} N_{\rm cP} \sigma_{\rm A}^2 \hat{\Gamma}^2(q, a_{\rm A}) P(q) \right)$$
(11)

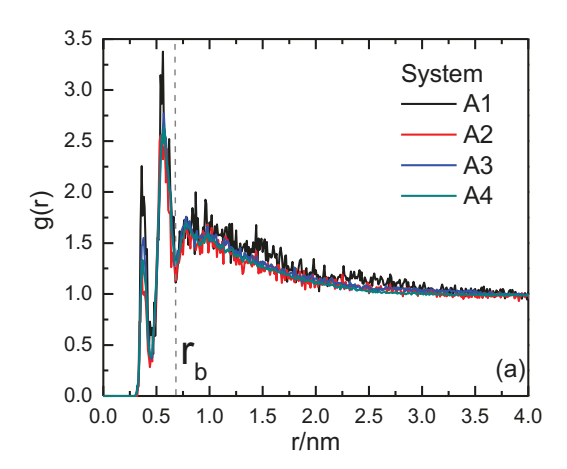
is the square of a wavenumber (q)-dependent inverse Debye length. ⁴³ The wavenumber q is normalized by the reference length $\ell = v_{\rm W}^{-1/2}$, and $l_{\rm B} = -\frac{2}{4\pi\epsilon_0\epsilon k_{\rm B}T}$ is the Bjerrum length, with ϵ_0 the permittivity of space, the unit of charge, and ϵ the dielectric constant of the medium, which we take to be that of water $(\epsilon = -)$. $\sigma_{\rm A}$ is the fraction of unpaired charged monomers of polyelectrolyte, calculated as $\sigma_{\rm A} = 1 - \alpha_{\rm AS}$. The normalized volume of a monomer $\omega_{\rm A} = v_{\rm A}/v_{\rm B}$ is calculated from the radius of a monomer $a_{\rm A}$, using $v_{\rm A} = -\pi a_{\rm A}$ which in turn is determined from the first peak of $g_{\rm CP-CP}(r)$ for a single fully charged chain (i.e., system C1, C2, or C3), so that $a_{\rm A}$ is the average distance between adjacent charged monomers on the chain, and has a value of $a_{\rm A} = 3.8$ ($n_{\rm A}$). We note that the salt size $a_{\rm A}$ is obtained from the volume $v_{\rm A} = \frac{4}{3}\pi a_{\rm A}^3$ of a salt ion,

which is obtained from $\omega_S = v_S/v$, whose value can be taken to be unity, as discussed below. The Gaussian smearing function in q space, $\hat{\Gamma}(q, a_i) = \exp\left(-\frac{1}{2}q^2a_i^2\right)$, appearing in the expressions for \tilde{k}^2 and μ_{AS}^{corr} , spreads the charge on salt ions and charged monomers across their size, a_i .^{43,58}

3. Results and Discussion

For the sake of simplicity, in the theory we here assume that the salt ion size is the same as that of a water molecule (i.e., $\omega_S = 1$) so that $\phi_S^f = M_S^f$ and the left-hand side of the theoretical equilibrium constant in Equation (8A), i.e., $\mathcal{K}_{theory} = \frac{\alpha_{AS}}{(1-\alpha_{AS})\,\phi_S^f}$, becomes identical to \mathcal{K}_{MD} in Equation (7). In the SI, we show that the effect of ion size can be simply embedded in ΔG_{AS} , without significantly changing the binding behavior of ions.

We first focus on short PAA chains (i.e., systems A1-A4), each of length five monomers, only one of which is charged. The binding of potassium ion to the PAA charged monomer is affected by chemical specificity, represented in the MD simulations by the Lennard Jones (LJ) parameters and partial charges of the monomers atoms, and the K⁺ ion. The ion-charged monomer RDF, g(r), exhibits distinct first and second peaks (see Figure 2a), corresponding to contact of the bare ion and the solvated ion, respectively, with the monomer. Noting the sharpness of these peaks, we define "bound" ions to be those within the area encompassed by the two, i.e., inside the dashed line at the minimum just beyond the second peak (r = r) in Figure 2a, while those beyond this distance are considered to be "free". (To be precise, in the MD simulations, first free ions are determined which are at least r distance away from each and every (charged) monomer, and then bound ions are determined.) Assuming an equilibrium exchange between bound and free ions according to Equation (3) and using their concentrations computed from the simulations, we use Equation (7A) to compute the equilibrium constant, \mathcal{K}_{MD} , and the free energy $\Delta G_{\text{AS}}^{\text{eff}}$ (= $-k_B T \ln \mathcal{K}_{\text{MD}}$) of potassium-monomer binding.



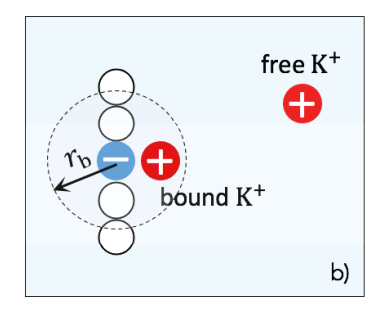


Figure 2. (a) Radial distribution functions, g(r), between the centers of mass of charged monomers and K⁺ for PAA chains with 5 monomers, with 5, 10, 20, and 30 chains in the simulation box, for systems A1 through A4. The dashed vertical line denotes the position of the second minimum of g(r) and defines the boundary between "bound" and "free" ions. (b) Schematic diagram defining the "bound" K⁺, where K⁺s close to the two partially negatively charged oxygen atoms of the charged monomer (i.e., the carboxyl group-containing monomer represented by the blue sphere) are responsible for

the first peak of g(r). Note that r in g(r) is the distance of a potassium ion from the center of mass of the monomer containing the charged carboxyl group.

As can be seen in Table 2, the binding free energies $\Delta G_{\rm AS}^{\rm eff}$ ($\approx -4.0~k_{\rm B}T$) for systems A1-A4 are nearly independent of the number of short chains in the box. Thus, the solution can be regarded as sufficiently dilute in charged monomer concentration that one can take the calculated $\Delta G_{\rm AS}^{\rm eff}$ to be the "intrinsic" binding free energy (i.e., $\mu_{\rm AS}^{\rm corr} \approx 0$ and $\Delta G_{\rm AS}^{\rm eff} \to \Delta G_{\rm AS} - 1$; see Equations 8A and 8B). Hence, $\Delta G_{\rm AS}^{\rm eff} = -4~k_{\rm B}T$ for the singly charged chains and $\Delta G_{\rm AS} = -3~k_{\rm B}T$.

Table 2 The effective free energy and its standard deviation (SD) calculated from MD simulation for the short 5-monomer PAA chains. The SD is obtained by dividing the simulation trajectory into 10 parts and taking $\Delta G_{\rm AS}^{\rm eff}$ from each part as an independent measure.

System	$\Delta G_{\mathrm{AS}}^{\mathrm{eff}}\left(k_{\mathrm{B}}T\right)$	SD
A1	-3.98	0.70
A2	-3.98	0.15
A3	-4.05	0.18
A4	-4.06	0.05

Now, we explore the longer, 30-monomer PAA chain with varying charge fractions (i.e., systems B and C1). It is well-established that the chain conformation of a polyelectrolyte transitions from a coil at low charge fraction (characteristic of neutral polymers) into an extended "rod-like" conformation at high charge fraction. The root mean-square of the end-to-end distance of the long PAA chain $\langle R_e^2 \rangle^{1/2}$, calculated from MD simulations, is plotted in Figure 3a. At the lowest charge fraction of the chain (B1: $\gamma = 0.1$), the PAA chain adopts a coil configuration with $\langle R_e^2 \rangle^{1/2} \approx 2.0 \, n$ (see the snapshot in Figure 3b). As the charge fraction increases, the chain expands by increasing its end-to-end distance, adopting a rod-like conformation at the highest charge fraction (C1: $\gamma = 1.0$; see Figure 3b), where the fully-extended length of a PAA chain with 30 monomers is around 7.6 nm. This chain conformation transitions to an extended state to lower the electrostatic repulsion between the COO⁻ groups. The electrostatic repulsions are also relieved by potassium binding to the chain, as discussed shortly.

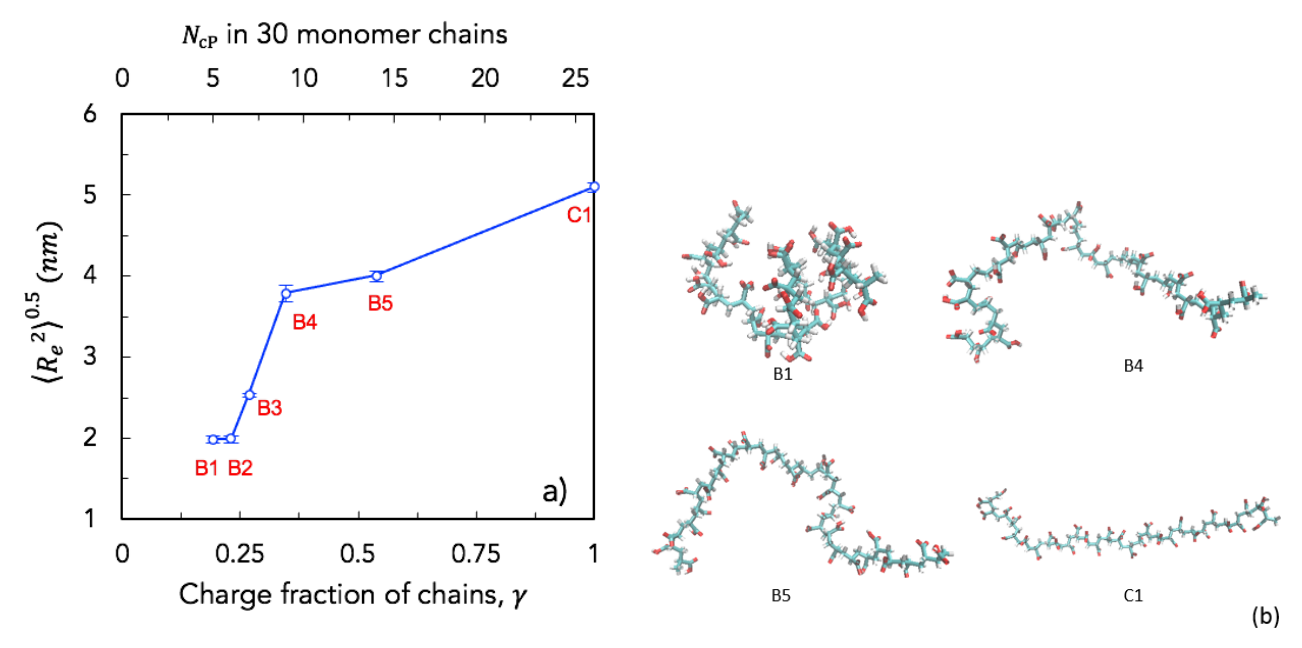


Figure 3. (a) Root mean square end-to-end distance, $\langle R_e^2 \rangle^{1/2}$, and (b) example chain conformations of the 30-monomer PAA chain with various charge fractions γ (or equivalently, number of charged monomers $N_{\rm cP}$): 0.19 (B1), 0.23 (B2), 0.27 (B3), 0.35 (B4), 0.54 (B5) and 1.0 (C1). Water molecules and counterions are not shown; shown are carboxylic acid hydrogen (white), oxygen (red), and aliphatic backbone carbon (cyan) atoms. Note in this and subsequent figures that the final two monomers at each end of the chain are kept neutral and these monomers are not included in definition of γ .

Figure 4a shows the radial distribution functions g(r) for potassium around charged monomers of the 30-monomer chain for varying charge fractions, where, as in Figure 2a, there are two distinct peaks. As the charge fraction along the chain decreases, the distribution of potassium ions around the charged groups approaches that for singly charged short 5-monomer chains (see Figure 4b). The g(r) peaks for the 30-monomer chain with the lowest charge fraction of the 30-monomer chain with (B1: $\gamma = 0.1$) almost matches that of the 5-monomer chains (Figure 4b).

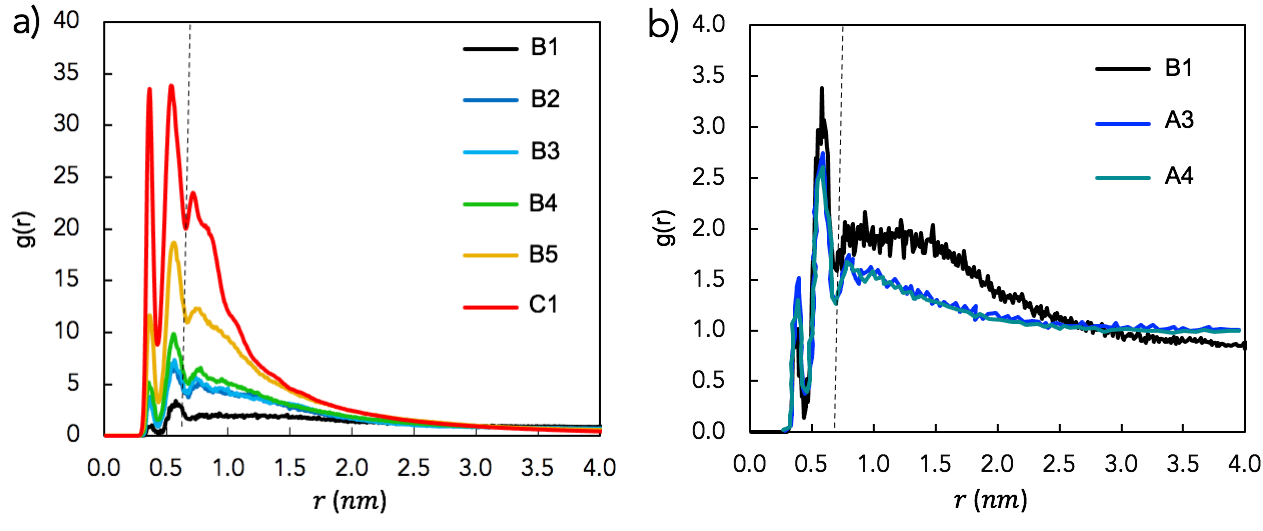


Figure 4. (a) Radial distribution functions, g(r), between the charged monomers and K+ for PAA chains with 30 monomers and various PAA charge fractions from $\gamma=0.1$ (system B1) to unity (system C1); see Table 1 for the specifications of each system. The dashed line denotes the location of the second minimum of g(r). (b) The radial distribution functions for K+ and the charged monomers in singly-charged short PAA chains with 20 and 30 chains in the simulation box, corresponding to systems A3 and A4, respectively. The black curve in (b) is for 30 monomer PAA chain with the charge fraction of $\gamma=0.1$ (system B1).

As the charge fraction along the chain increases, the two peaks of g(r) grow strongly. This shows that potassium ions more strongly localize and bind to the charged monomers of the chain as the charge fraction increases.

Next, to quantify the binding of potassium ions, we use the same criterion to distinguish free and bound ions as in short-chain systems; the ions at distances from a charged monomer up to the second minimum in g(r) (i.e., the dashed line in Figure 4a) are considered to be bound. Then, using the concentrations of free and bound potassium ions, one can employ Equation 7A to calculate the equilibrium constant and from this the effective binding free energy ΔG_{AS}^{eff} from the MD simulations, which are shown in Figure 5. As can be seen, ΔG_{AS}^{eff} almost equals that in singly charged, short chains ($\Delta G_{AS}^{eff} \approx -4 k_B T$) at the lowest charge fraction of the chain (with $\gamma = 0.1$). Evidently in this limit, the binding of potassium ions to the charged monomers of the long chain are nearly uncorrelated with each other, as inferred from Figure 4b. However, at high charge fractions, the ion binding to the charged monomers strengthens greatly, resulting in larger g(r) peaks in Figure 4a and hence, a greater fraction of bound ions to the charged monomers, α_{AS} , in Figure 5a.

To test our theory for ion binding to PE chains, we use Equations 8A and 8B to find the binding equilibrium constant and effective free energy. Briefly, using the intrinsic binding free energy, $\Delta G_{AS}(=-3 k_B T)$ taken from the singly-charged short chains, and a form factor for the PAA chain configuration, we calculate the binding fraction from Equation 8A and effective free energy from Equation 8B. The contribution of electrostatic correlations to ion binding is calculated within the RPA using Equation 9. To approximate the chain form factor, we either use a predefined form factor (either a rod or a Gaussian coil), or the form factor of the 30-monomer chain from MD simulations (using Equations 10A or 10B). For the rod form factor, the length of the chain is set at $L_r \approx 26a_A$ (with $a_A = 0.38 n$ being the diameter of a monomer; see Figure S1), while the Kuhn length of the Gaussian coil was assumed to be the monomer diameter for simplicity, giving a radius of gyration of $R_g \approx \left(\frac{26\alpha_A^2}{6}\right)^{0.5} = 2.5 \, n$. Note that the two final monomers at each end of the chain do not contribute to electrostatic correlations, so their effect is removed from chain form factors. The predictions of the theory in Figure 5 qualitatively resemble the MD results, with predictions of the rodlike form factor and from the MD simulations agreeing better than those from the Gaussian form factor. The Gaussian coil form factor leads to stronger repulsions along the chain than for the rod form factor, which are relieved by attracting ions more strongly to the coil (i.e., more negative ΔG_{AS}^{eff} in Figure 5b), yielding higher fractions of bound ions (i.e., higher α_{AS} in Figure 5a).

At low charge fractions on the 30-monomer PAA chain, the MD results disagree more strongly from the predictions, regardless of the method of prescribing the chain structure. However, upon increase of the charge fraction, the model predictions for a form factor of a rod, or taken from the MD simulations using either Equation 10A or 10B, agree semi-quantitatively with the results of the MD simulations for α_{AS} and ΔG_{AS}^{eff} . (The charged monomer-charged monomer RDFs used to obtain the form factor in Equation 10A are given in Figure S1.) Figure 5 shows that the contribution of electrostatic correlations to ion binding, μ_{AS}^{corr} , nicely captures the increased strength of potassium binding needed to relieve the high electrostatic repulsions along a highly charged chain. The more accurate predictions from the rod form factor than the Gaussian one at high

charge fractions is consistent with the extended PAA configurations at high charge fractions depicted in Figure 3b.

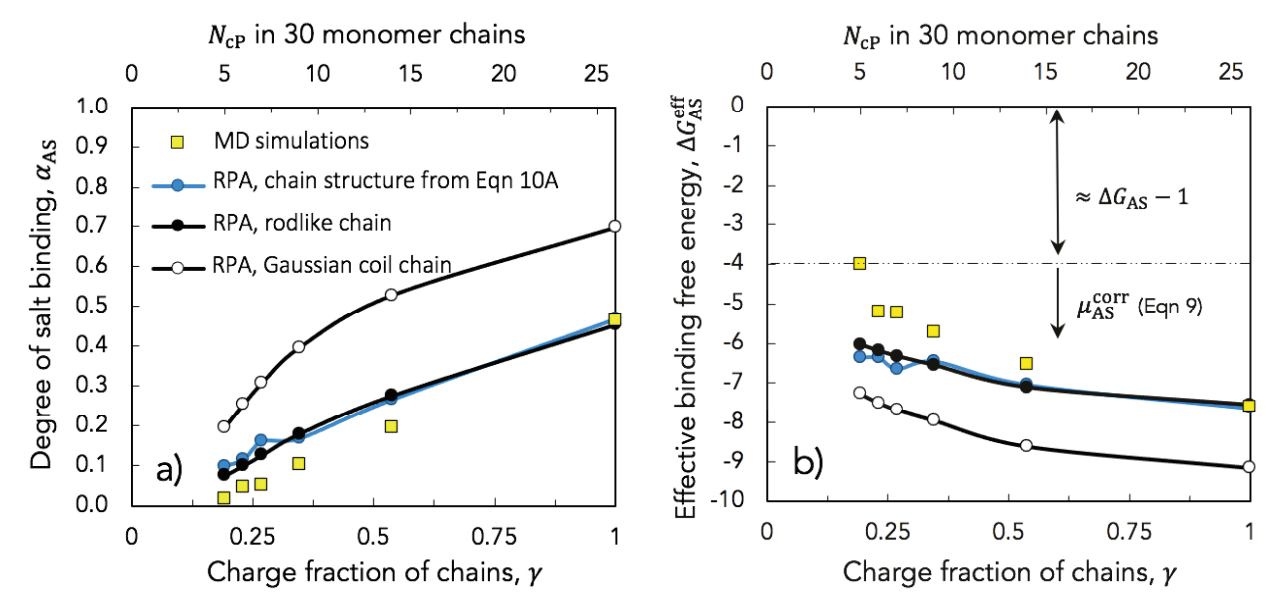


Figure 5. Comparison of a) the binding fraction $\alpha_{\rm AS}$ and b) effective binding free energy $\Delta G_{\rm AS}^{\rm eff}$ (in units of $k_{\rm B}T$) as functions of the charge fraction γ (or equivalently, number of charged monomers $N_{\rm cP}$) of 30-monomer PAA chains, from MD simulations and theory. Note in this and other figures that the final two monomers at each end of the chain are kept neutral and these monomers are not included in definitions of $\alpha_{\rm AS}$ and γ . The contributions to the effective binding free energy $\Delta G_{\rm AS}^{\rm eff} = \Delta G_{\rm AS} + \mu_{\rm AS}^{\rm corr} - 1$ beyond $\Delta G_{\rm AS} - 1 = -4 \ k_{\rm B}T$ are due to the electrostatic correlations, given by $\mu_{\rm AS}^{\rm corr}$ (Equation 9). The coupling of binding free energy $\Delta G_{\rm AS}^{\rm eff}$ and fraction of binding $\alpha_{\rm AS}$ is given by Equation 8. Predictions using the form factor from Equation 10B are given in Figure S2.

Next, we investigate the neutralization of fully charged PAA chains (systems C1-C3) as a function of its degree of polymerization. Figure S3 shows that in both MD simulations and theory, increasing the degree of polymerization of the "fully charged" chains from 30 to 56 slightly increases the binding fraction α_{AS} and the binding strength, $|\Delta G_{AS}^{eff}|$. As in Figure 5, the intrinsic binding free energy, ΔG_{AS} , was set at $-3~k_BT$ in the theory.

Interestingly, however, the rate of change of α_{AS} and $|\Delta G_{AS}^{eff}|$ with the length of (fully charged) chains is much slower than with the charge fraction γ at fixed chain length (see Figure 6 which merges plots of Figures 5 and S3). It can be concluded that the electrostatic repulsions between nearest adjacent charged monomers have a much stronger effect on ion binding than do the repulsions between non-adjacent charged monomers.

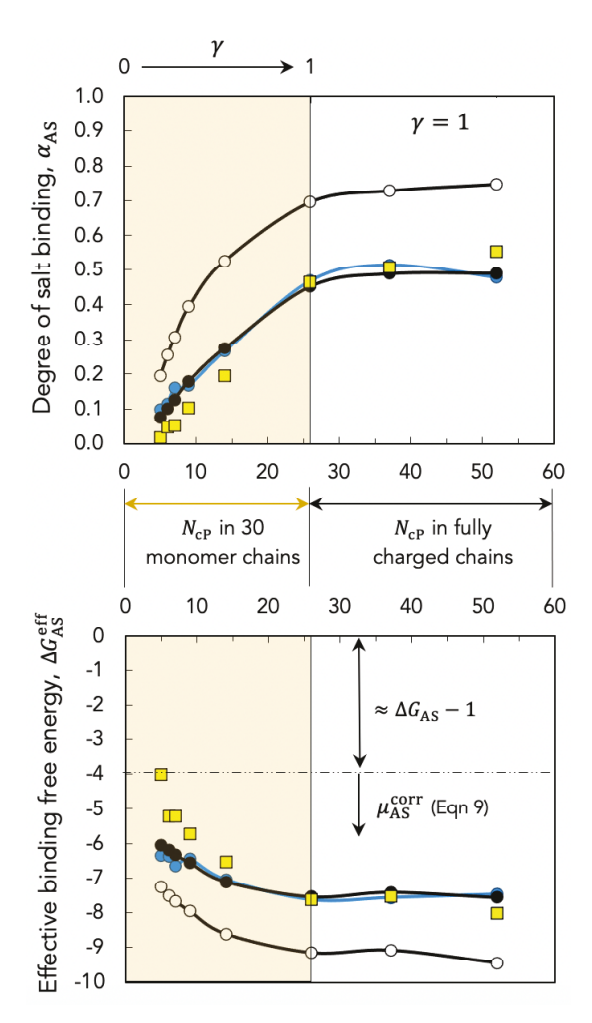


Figure 6. a) Binding fraction α_{AS} and b) effective binding free energy ΔG_{AS}^{eff} (in units of k_BT) for 30-monomer PAA chains with varying charge fraction (in the yellow-shaded region) and for fully charged PAA chains with varying chain length (in the white-shaded region). The legend is the same as in Figure 5. Note that the final two monomers at each end of each chain are kept neutral and are not included in definitions of α_{AS} and γ . The contributions to the effective binding free energy $\Delta G_{AS}^{eff} = \Delta G_{AS} + \mu_{AS}^{corr} - 1$ beyond $\Delta G_{AS} - 1 = -4 k_B T$ is due to the electrostatic correlations, given by μ_{AS}^{corr} (Equation 9). The coupling of binding free energy ΔG_{AS}^{eff} and fraction of binding α_{AS} is given by Equation 8.

Finally, we note that the ion size can affect its binding behavior, as discussed in our previous study.⁵⁵ In Figure S4 of the SI, we present the results when hydration numbers of potassium ions are taken into account, which increases the (effective) size of the ion, ω_S . The results in Figure S4 closely mimic those in Figure 6, with the difference that the increase of ion size ω_S mainly just shifts the intrinsic binding free energy ΔG_{AS} (and therefore $\Delta G_{AS}^{\text{eff}}$) to more positive values. Note that if ΔG_{AS} is kept fixed, upon increase of ω_S , the mixing entropy of the ions decreases, and this leads to more extensive binding of ions to polyelectrolytes.⁵⁵

4. Conclusions and Prospective

We studied neutralization of poly(acrylic acid), or PAA, chains by potassium ions using MD simulations and theory. Three types of simulation systems were investigated: A) a box containing a few short, singly-charged chains, B) a box containing a longer (30-monomer) chain with various numbers of charged monomers (or equivalently, with various charge fractions), and C) a box containing a nearly fully charged chain with different lengths (\geq 30 monomers). Each system contains potassium ions as the counterions of PAA. We extracted free

energies of binding of potassium ions to PAA chain, ΔG_{AS}^{eff} , using the ion-charged monomer radial distribution function (RDF) for each of the aforementioned systems. It was found that the potassium binding free energy for type A systems does not change with the number of singly-charged chains ($\Delta G_{AS}^{eff} \approx \text{constant}$), and hence, one can in this case regard it as the *intrinsic* free energy of potassium-carboxylic group binding ($\Delta G_{AS}^{eff} \approx \Delta G_{AS}$). Interestingly, this binding free energy matches that of the 30-monomer chain at the lowest charge fraction in the type B systems. However, as the charge fraction of the chain in type B systems increases, the chain adopts a more extended configuration. Simultaneously, ΔG_{AS}^{eff} becomes more negative, corresponding to stronger potassium-PAA binding, and therefore, a higher degree of potassium binding to the chain, α_{AS} .

Next, we used the intrinsic binding free energy ΔG_{AS} obtained as described above as input to test the ability of our theory to predict salt ion binding to polyelectrolyte chains, including the effects of ion proximity along the chain. Our theory is based on a mass action equation that dictates an equilibrium exchange between free ions and ions bound to PE chains. The (effective) free energy of ion binding to PE chains ΔG_{AS}^{eff} has two contributions: the intrinsic free energy, ΔG_{AS} , and the electrostatic correlations μ_{AS}^{corr} , where the latter is obtained from a random phase approximation (RPA). $\mu_{\rm AS}^{\rm corr}$ in turn strongly depends on chain configuration and the correlations among charged monomers in the chain. Interestingly, we find that using the intrinsic ΔG_{AS} obtained from singly-charged chains, and a rodlike chain configuration or a configuration directly from MD simulations, the theory yields semi-quantitative predictions for ΔG_{AS}^{eff} and α_{AS} as a function of charge fraction without using any fitting parameter. The accuracy of the predictions improves at higher charge fractions of PAA chains (i.e., systems B and C). This suggests that a combination of intrinsic binding free energy, which captures chemical specificity of charged species, and RPA, which accounts for the effects of chain configuration and polyelectrolyte charge fraction on electrostatic correlations, provides reliable predictions of neutralization of polyelectrolytes by salt ions. An extension of this theory may be able to predict more complex phenomena such as ion pairing, by obtaining intrinsic binding free energies of ion pairing from analogous molecular dynamics simulations.

Acknowledgments

This work was supported by the National Science Foundation under Grant No. 1707640. W. Tian acknowledges financial support from Jiangsu Overseas Visiting Scholar Program for University Prominent Young and Mid-aged Teachers and Presidents (2019), PAPD of Jiangsu Higher Education Institutions.

References

- Kroschwald, S., Maharana, S., Mateju, D., Malinovska, L., Nüske, E., Poser, I., Richter, D. & Alberti, S. Promiscuous Interactions and Protein Disaggregases Determine the Material State of Stress-Inducible RNP Granules. *eLife* 4, e06807 (2015).
- 2. Banani, S. F., Lee, H. O., Hyman, A. A. & Rosen, M. K. Biomolecular Condensates: Organizers of Cellular Biochemistry. *Nature Reviews Molecular Cell Biology* **18**, 285–298 (2017).

- 3. Nakashima, K. K., Vibhute, M. A. & Spruijt, E. Biomolecular Chemistry in Liquid Phase Separated Compartments. *Frontiers in molecular biosciences* **6**, 21 (2019).
- 4. Shakya, A., Park, S., Rana, N. & King, J. T. Liquid-Liquid Phase Separation of Histone Proteins in Cells: Role in Chromatin Organization. *Biophysical Journal* **118**, 753–764 (2020).
- 5. Lu, T. & Spruijt, E. Multiphase Complex Coacervate Droplets. *Journal of the American Chemical Society* **142**, 2905–2914 (2020).
- Garmann, R. F., Goldfain, A. M. & Manoharan, V. N. Measurements of the Self-Assembly Kinetics of Individual Viral Capsids Around Their RNA Genome. *Proceedings of the National Academy of Sciences* 116, 22485 LP – 22490 (2019).
- 7. Felgner, P. L., Gadek, T. R., Holm, M., Roman, R., Chan, H. W., Wenz, M., Northrop, J. P., Ringold, G. M. & Danielsen, M. Lipofection: A Highly Efficient, Lipid-Mediated DNA-Transfection Procedure. *Proceedings of the National Academy of Sciences* 84, 7413–7417 (1987).
- 8. Mi, X., Blocher McTigue, W. C., Joshi, P. U., Bunker, M. K., Heldt, C. L. & Perry, S. L. Thermostabilization of Viruses via Complex Coacervation. *Biomaterials Science* (2020). doi:10.1039/D0BM01433H
- 9. Blocher, W. C. & Perry, S. L. Complex Coacervate-Based Materials for Biomedicine. *WIREs Nanomedicine and Nanobiotechnology* **9**, e1442 (2017).
- 10. Kapelner, R. A. & Obermeyer, A. C. Ionic Polypeptide Tags for Protein Phase Separation. *Journal of Chemical Sciences* **10**, 2700–2707 (2019).
- 11. Shamoun, R. F., Reisch, A. & Schlenoff, J. B. Extruded Saloplastic Polyelectrolyte Complexes. *Advanced Functional Materials* **22**, 1923–1931 (2012).
- 12. Alkekhia, D., Hammond, P. T. & Shukla, A. Layer-by-Layer Biomaterials for Drug Delivery. *Annual Review of Biomedical Engineering* **22**, 1–24 (2020).
- 13. Barberio, A. E., Smith, S. G., Correa, S., Nguyen, C., Nhan, B., Melo, M., Tokatlian, T., Suh, H., Irvine, D. J. & Hammond, P. T. Cancer Cell Coating Nanoparticles for Optimal Tumor-Specific Cytokine Delivery. *ACS nano* **14,** 11238–11253 (2020).
- 14. Kazemabad, M., Verliefde, A., Cornelissen, E. R. & D'Haese, A. Crown Ether Containing Polyelectrolyte Multilayer Membranes for Lithium Recovery. *Journal of Membrane Science* **595**, 117432 (2020).
- 15. Schlenoff, J. B. & Dubas, S. T. Mechanism of Polyelectrolyte Multilayer Growth: Charge Overcompensation and Distribution. *Macromolecules* **34**, 592–598 (2001).
- 16. Debye, P. & Hückel, E. Zur Theorie der Elektrolyte. *Physikalische Zeitschrift* **9**, 185–206 (1923).
- 17. Shen, K. & Wang, Z.-G. Electrostatic Correlations and the Polyelectrolyte Self Energy. *The Journal of Chemical Physics* **146**, 84901/1–16 (2017).
- 18. Qin, J. & de Pablo, J. J. Criticality and Connectivity in Macromolecular Charge Complexation. *Macromolecules* **49,** 8789–8800 (2016).
- 19. Overbeek, J. T. G. & Voorn, M. J. Phase Separation in Polyelectrolyte Solutions. Theory of Complex Coacervation. *Journal of Cellular and Comparative Physiology* **49**, 7–26 (1957).
- Park, S., Barnes, R., Lin, Y., Jeon, B., Najafi, S., Delaney, K. T., Fredrickson, G. H., Shea, J.-E., Hwang, D. S. & Han, S. Dehydration Entropy Drives Liquid-Liquid Phase Separation by Molecular Crowding.
 Communications Chemistry 3, 83 (2020).
- 21. McCarty, J., Delaney, K. T., Danielsen, S. P. O., Fredrickson, G. H. & Shea, J.-E. Complete Phase Diagram for Liquid–Liquid Phase Separation of Intrinsically Disordered Proteins. *The Journal of Physical Chemistry Letters* **10**, 1644–1652 (2019).
- 22. Danielsen, S. P. O., McCarty, J., Shea, J.-E., Delaney, K. T. & Fredrickson, G. H. Molecular Design of Self-Coacervation Phenomena in Block Polyampholytes. *Proceedings of the National Academy of Sciences* 116,

- 8224-8232 (2019).
- 23. Borue, V. Y. & Erukhimovich, I. Y. A Statistical Theory of Weakly Charged Polyelectrolytes: Fluctuations, Equation of State and Microphase Separation. *Macromolecules* **21**, 3240–3249 (1988).
- 24. Hostnik, G., Podlipnik, Č., Mériguet, G. & Cerar, J. Specificity of Counterion Binding to a Conjugated Polyelectrolyte: A Combined Molecular Dynamics and NOESY Investigation. *Macromolecules* **53**, 1119–1128 (2020).
- Hinderberger, D., Spiess, H. W. & Jeschke, G. Dynamics, Site Binding, and Distribution of Counterions in Polyelectrolyte Solutions Studied by Electron Paramagnetic Resonance Spectroscopy. *The Journal of Physical Chemistry B* 108, 3698–3704 (2004).
- 26. Hori, N., Denesyuk, N. A. & Thirumalai, D. Ion Condensation onto Ribozyme Is Site Specific and Fold Dependent. *Biophysical Journal* **116**, 2400–2410 (2019).
- 27. Ghostine, R. A., Shamoun, R. F. & Schlenoff, J. B. Doping and Diffusion in an Extruded Saloplastic Polyelectrolyte Complex. *Macromolecules* **46**, 4089–4094 (2013).
- 28. Salomäki, M., Tervasmäki, P., Areva, S. & Kankare, J. The Hofmeister Anion Effect and the Growth of Polyelectrolyte Multilayers. *Langmuir* **20**, 3679–3683 (2004).
- 29. Wandrey, C., Hunkeler, D., Wendler, U. & Jaeger, W. Counterion Activity of Highly Charged Strong Polyelectrolytes. *Macromolecules* **33**, 7136–7143 (2000).
- 30. Hofmeister, F. Zur Lehre von der Wirkung der Salze. *Archiv für experimentelle Pathologie und Pharmakologie* **24,** 247–260 (1888).
- 31. Manning, G. S. Limiting Laws and Counterion Condensation in Polyelectrolyte Solutions I. Colligative Properties. *The Journal of Chemical Physics* **51**, 924–933 (1969).
- 32. Manning, G. S. Limiting Laws and Counterion Condensation in Polyelectrolyte Solutions II. Self-Diffusion of the Small Ions. *The Journal of Chemical Physics* **51**, 934–938 (1969).
- 33. Manning, G. S. Counterion Binding in Polyelectrolyte Theory. *Accounts of Chemical Research* **12**, 443–449 (1979).
- 34. Batys, P., Luukkonen, S. & Sammalkorpi, M. Ability of the Poisson–Boltzmann Equation to Capture Molecular Dynamics Predicted Ion Distribution Around Polyelectrolytes. *Physical Chemistry Chemical Physics* **19**, 24583–24593 (2017).
- 35. Muthukumar, M. Theory of Counter-Ion Condensation on Flexible Polyelectrolytes: Adsorption Mechanism. *The Journal of Chemical Physics* **120**, 9343–9350 (2004).
- 36. Hua, J., Mitra, M. K. & Muthukumar, M. Theory of Volume Transition in Polyelectrolyte Gels with Charge Regularization. *The Journal of Chemical Physics* **136**, 134901 (2012).
- 37. Madinya, J. J., Chang, L.-W., Perry, S. L. & Sing, C. E. Sequence-Dependent Self-Coacervation in High Charge-Density Polyampholytes. *Mol. Syst. Des. Eng.* **5**, 632–644 (2020).
- Liu, Y., Santa Chalarca, C. F., Carmean, R. N., Olson, R. A., Madinya, J., Sumerlin, B. S., Sing, C. E., Emrick, T. & Perry, S. L. Effect of Polymer Chemistry on the Linear Viscoelasticity of Complex Coacervates.
 Macromolecules 53, 7851–7864 (2020).
- 39. Lytle, T. K., Chang, L.-W., Markiewicz, N., Perry, S. L. & Sing, C. E. Designing Electrostatic Interactions via Polyelectrolyte Monomer Sequence. *ACS Central Science* **5**, 709–718 (2019).
- 40. Lytle, T. K. & Sing, C. E. Transfer Matrix Theory of Polymer Complex Coacervation. *Soft Matter* **13**, 7001–7012 (2017).
- 41. Lytle, T. K., Salazar, A. J. & Sing, C. E. Interfacial Properties of Polymeric Complex Coacervates from Simulation and Theory. *The Journal of Chemical Physics* **149**, 163315 (2018).
- 42. Ermoshkin, A. V & Olvera de la Cruz, M. A Modified Random Phase Approximation of Polyelectrolyte

- Solutions. *Macromolecules* **36**, 7824–7832 (2003).
- 43. Friedowitz, S., Salehi, A., Larson, R. G. & Qin, J. Role of Electrostatic Correlations in Polyelectrolyte Charge Association. *The Journal of Chemical Physics* **149**, 163335/1–14 (2018).
- 44. Salehi, A. & Larson, R. G. A Molecular Thermodynamic Model of Complexation in Mixtures of Oppositely Charged Polyelectrolytes with Explicit Account of Charge Association/Dissociation. *Macromolecules* **49**, 9706–9719 (2016).
- 45. Lou, J., Friedowitz, S., Qin, J. & Xia, Y. Tunable Coacervation of Well-Defined Homologous Polyanions and Polycations by Local Polarity. *ACS Central Science* **5**, 549–557 (2019).
- 46. Ghasemi, M. & Larson, R. G. Role of Electrostatic Interactions in Charge Regulation of Weakly Dissociating Polyacids. *Progress in Polymer Science* **112**, 101322 (2021).
- 47. Hinderberger, D., Jeschke, G. & Spiess, H. W. Counterion Condensation and Conformational Transitions of Polyelectrolytes Characterized by EPR Spectroscopy. *Macromolecules* **35**, 9698–9706 (2002).
- 48. Abraham, M. J., Murtola, T., Schulz, R., Páll, S., Smith, J. C., Hess, B. & Lindahl, E. GROMACS: High Performance Molecular Simulations Through Multi-Level Parallelism from Laptops to Supercomputers. *SoftwareX* **1–2**, 19–25 (2015).
- 49. Wang, J., Wolf, R. M., Caldwell, J. W., Kollman, P. A. & Case, D. A. Development and Testing of A general Amber Force Field. *Journal of Computational Chemistry* **25**, 1157–1174 (2004).
- 50. Mintis, D. G. & Mavrantzas, V. G. Effect of pH and Molecular Length on the Structure and Dynamics of Short Poly(acrylic acid) in Dilute Solution: Detailed Molecular Dynamics Study. *The Journal of Physical Chemistry B* **123**, 4204–4219 (2019).
- 51. Nosé, S. A Molecular Dynamics Method for Simulations in the Canonical Ensemble. *Molecular Physics* **52**, 255–268 (1984).
- 52. Parrinello, M. & Rahman, A. Polymorphic Transitions in Single Crystals: A New Molecular Dynamics Method. *Journal of Applied Physics* **52**, 7182–7190 (1981).
- 53. Darden, T., York, D. & Pedersen, L. Particle Mesh Ewald: An N·log(N) Method for Ewald Sums in Large Systems. *The Journal of Chemical Physics* **98**, 10089–10092 (1993).
- 54. Hess, B. P-LINCS: A Parallel Linear Constraint Solver for Molecular Simulation. *Journal of Chemical Theory and Computation* **4**, 116–122 (2008).
- 55. Ghasemi, M., Friedowitz, S. & Larson, R. G. Analysis of Partitioning of Salt Through Doping of Polyelectrolyte Complex Coacervates. *Macromolecules* **53**, 6928–6945 (2020).
- 56. Bergsma, J., Leermakers, F. A. M., Kleijn, J. M. & van der Gucht, J. A Hybrid Monte Carlo Self-Consistent Field Model of Physical Gels of Telechelic Polymers. *Journal of Chemical Theory and Computation* **14**, 6532–6543 (2018).
- 57. Liu, H. & Paddison, S. J. Direct Calculation of the X-Ray Structure Factor of Ionic Liquids. *Physical Chemistry Chemical Physics* **18**, 11000–11007 (2016).
- 58. Wang, Z.-G. Fluctuation in Electrolyte Solutions: The Self Energy. *Physical Review E* **81**, 21501/1–12 (2010).

Supporting Information (SI)

Extracting Free Energies of Salt Ion Binding to Polyelectrolytes by Molecular Dynamics Simulations

Center for Soft Condensed Matter Physics and Interdisciplinary Research, Soochow University, Suzhou 215006, China Department of Chemical Engineering, University of Michigan, Ann Arbor, Michigan 48109

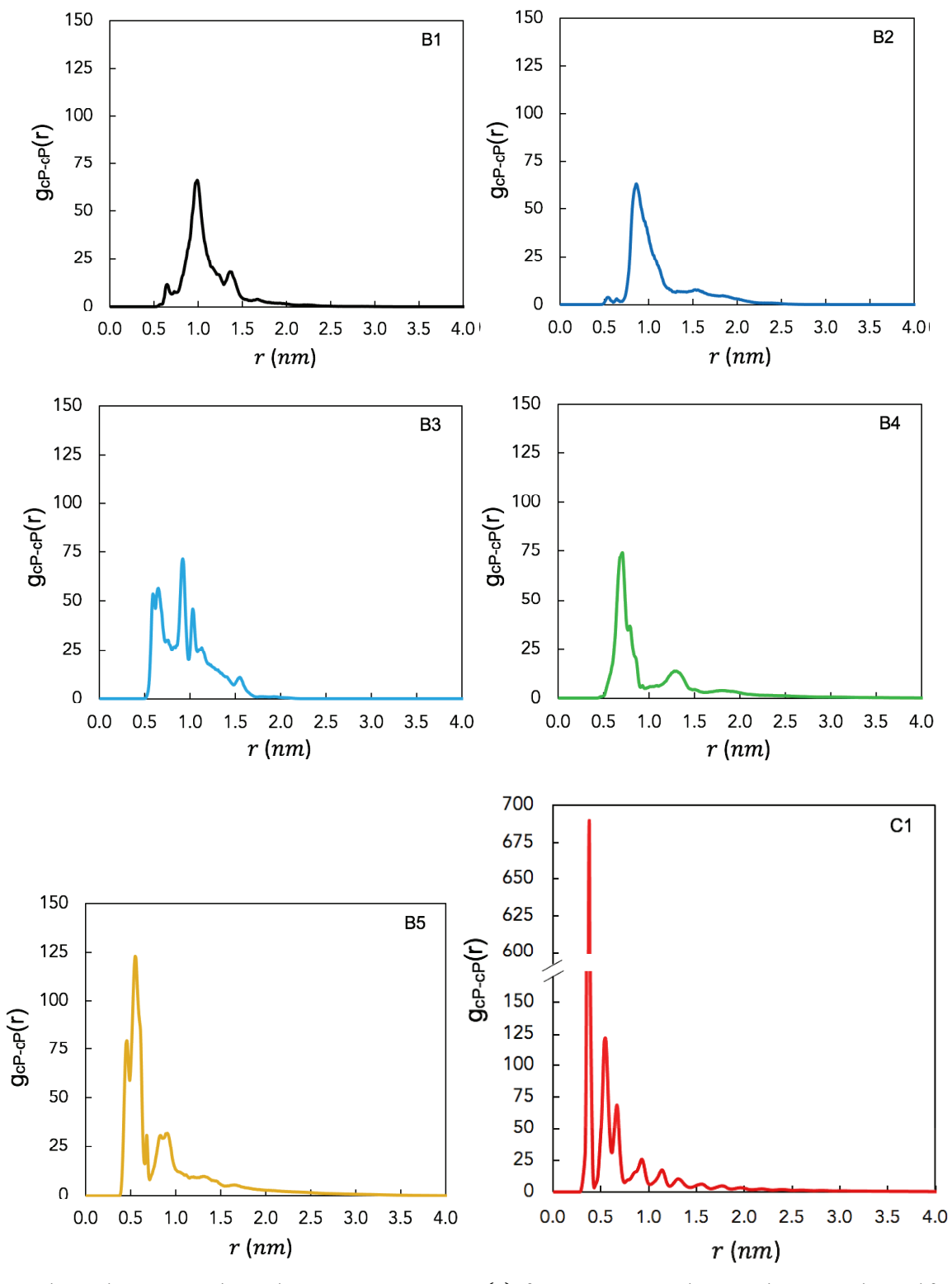


Figure S1. Charged monomer-charged monomer RDF, $g_{\rm cP-cP}(r)$, for 30-monomer chains with varying charged fractions from the MD simulations, as described in Table 1 of the main text. The first peak of system C1 ("fully" charged, 30-monomer chain) lies at a distance of $a_{\rm A} \approx 0.38~(n_{\rm c})$).

Table S1. The effective free energy and standard deviation (SD) calculated from MD simulation for systems of type B and C.

System	$\Delta G_{\rm AS}^{\rm eff} \left({}_{\rm B}T \right)$	SD of $\Delta G_{AS}^{\mathrm{eff}}$
B1	-3.91	1.50
B2	-5.20	0.55
В3	-5.22	0.47
B4	-5.73	0.52
B5	-6.54	0.23
C1	-7.61	0.11
C2	-7.53	0.12
C3	-8.02	0.07

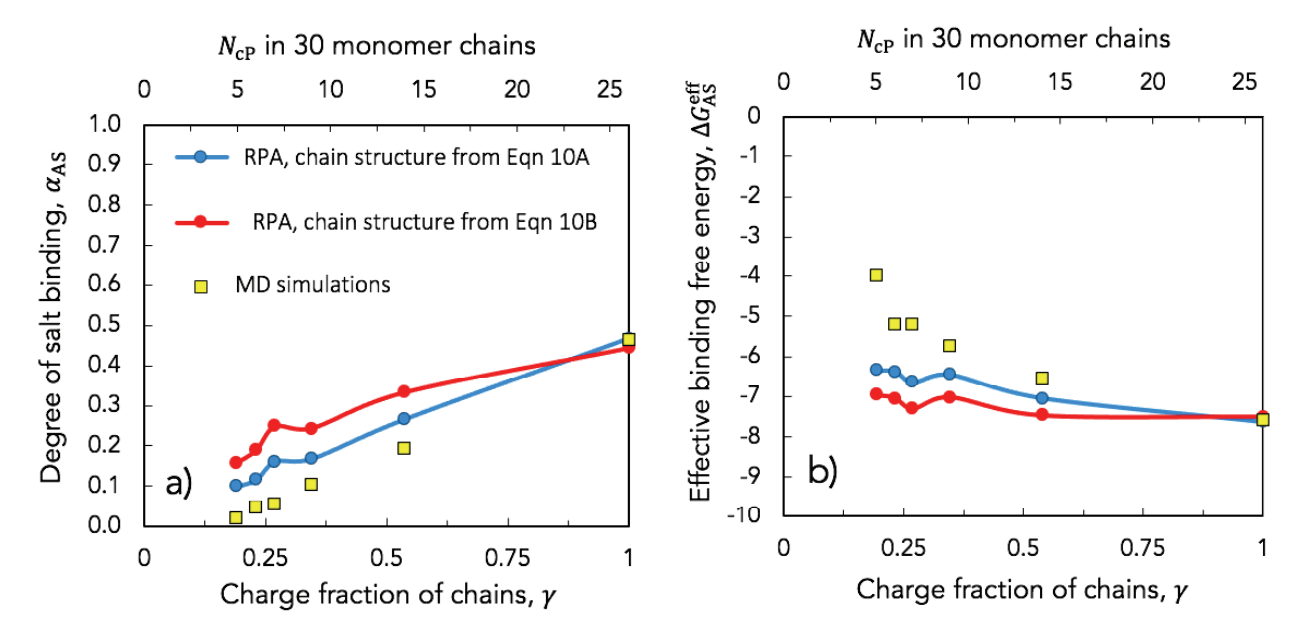
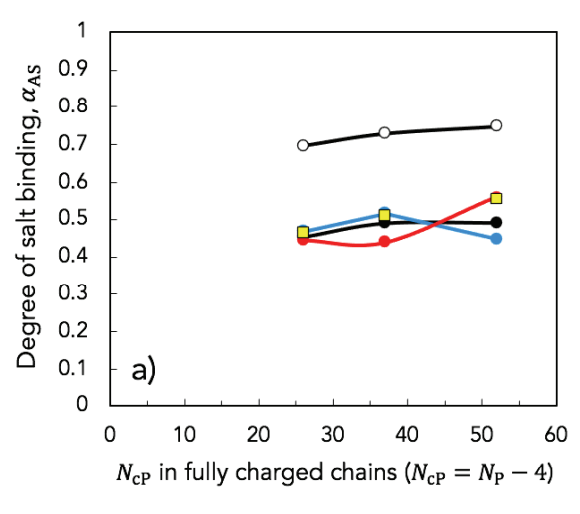


Figure S2. a) Binding fraction α_{AS} and b) effective binding free energy $\Delta G_{AS}^{\, {\rm eff}}$ (in units of $k_B T$) as functions of the charge fraction γ (or equivalently, number of charged monomers $N_{\rm cP}$) of 30-monomer PAA chains, from MD simulations and theory based on chain structure from the simulations, using Eqs. 10A and 10B in the main text. Note that two monomers at each end of the chain are kept neutral and these monomers are not included in definitions of α_{AS} .



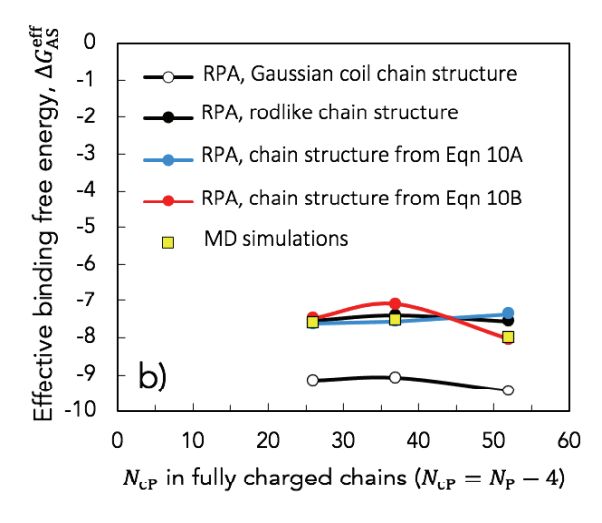


Figure S3. a) Binding fraction $\alpha_{\rm AS}$ and b) effective binding free energy $\Delta G_{\rm AS}^{\rm eff}$ (in units of $k_{\rm B}T$) as functions of the number of charged monomers along "fully" charged PAA ($N_{\rm cP}$), from MD simulations and theory. Note that two monomers at each end of the chain are kept neutral and these monomers are not included in definitions of $\alpha_{\rm AS}$. For the rod form factors, the length of the chain is set at $L_r \approx N_{\rm cP} a_{\rm A}$ (with $a_{\rm A}=0.38~n$ being the diameter of a monomer; see Figure S1), while the Kuhn length of the Gaussian coil was assumed to be the monomer diameter for simplicity, giving a radius of gyration of $R_g \approx \left(\frac{N_{\rm cP} a_{\rm A}^2}{6}\right)^{0.5}$.

Comparison of theoretical and simulation results for $\omega_S > 1$

Potassium ions carry on average three water molecules in their hydration shell (corresponding to $\omega_S = 3$), however, the number of hydration waters is sensitive on the technique used to measure it. To compare the theoretical and simulation results when $\omega_S > 1$, the equilibrium constant used to present the MD simulation results (i.e., Equation 7C) has to be changed so that it is consistent with theoretical equilibrium constant in Equation 8A. To do so, we simply multiply both sides of Equation 7C by ω_S ,

$$\mathcal{K}_{\text{MD,2}} = \frac{\mathcal{K}_{\text{M}}}{\omega_{\text{S}}} = \frac{[\text{MA-N}]}{[\text{MA-N}]} \frac{[\text{MA-N}]}{[\text{MA-N}]}$$

$$= \frac{\alpha_{\text{AS}}}{(1-\alpha_{\text{AS}})} \frac{\phi_{\text{S}}^{\text{f}}}{\phi_{\text{S}}^{\text{f}}}$$
(S1b)

As can be seen, Equation S1b is identical to the left-hand side of Equation 8A. Given that $\Delta G_{AS,2}^{eff} = -\ln \mathcal{K}_{MD,2}$, one can see that the effective binding free energies from the MD results simply shift by $\ln \omega_S$ when $\omega_S > 1$, i.e., $\Delta G_{AS,2}^{eff} = -\ln \mathcal{K}_{MD,2} = -\ln \mathcal{K}_{MD} + \ln \omega_S = \Delta G_{AS}^{eff} + \ln \omega_S$ where $\Delta G_{AS}^{eff} (= -\ln \mathcal{K}_{MD})$ are the effective binding free energies from the MD simulations for $\omega_S = 1$. Therefore, the simulation results for the box containing short chains (i.e., systems A1-A4) for $\omega_S = 3$ shift by $\ln 3.0 = +1.1$ ($k_B T$) (compared to those in Table 2) leading to $\Delta G_{AS,2}^{eff} \approx -2$ $k_B T$ for the ion size of $\omega_S = 3$ as follows,

Table S2. The effective free energy and its standard deviation (SD) calculated from MD simulation for the short 5-monomer PAA chains when $\omega_S=1$, giving $\Delta G_{AS}^{eff}=-\ln\mathcal{K}_{MD}$ (also presented in Table 2), and when $\omega_S=3$, and $\Delta G_{AS.2}^{eff}=-\ln\mathcal{K}_{MD,2}$.

System	$\Delta G_{\mathrm{AS}}^{\mathrm{eff}}\left(k_{\mathrm{B}}T\right)$	$\Delta G_{\mathrm{AS}}^{\mathrm{eff,2}}\left(k_{\mathrm{B}}T\right)$
A1	-3.98	-2.88
A2	-3.98	-2.88

A3	-4.05	-2.95
A4	-4.06	-2.96

Given that for singly-charged, short chains the electrostatic correlations play little role in potassium binding to PAA chains (i.e., $\Delta G_{AS,2}^{eff} \rightarrow \Delta G_{AS,2} - 1$), we find the intrinsic binding free energy to be $\Delta G_{AS,2} \approx -1$ k_BT . Similarly, the effective biding free energies at $\omega_S = 3$ for systems B1-B4 and C1-C3 simply shifts by $+1.1 k_BT$ compared to their equivalent values at $\omega_S = 1$ (see Figure S4).

Next, we use the intrinsic binding free energy $\Delta G_{\text{AS},2}$ and $\omega_{\text{S}}=3$ to find the predicted degree of potassium binding α_{AS} and effective binding free energy $\Delta G_{\text{AS},2}^{\text{eff}}$ from the theory. Plotted in Figure S4 are α_{AS} and $\Delta G_{\text{AS},2}^{\text{eff}}$ from the theory using various chain structures and also from the simulations for $\omega_{\text{S}}=3$,

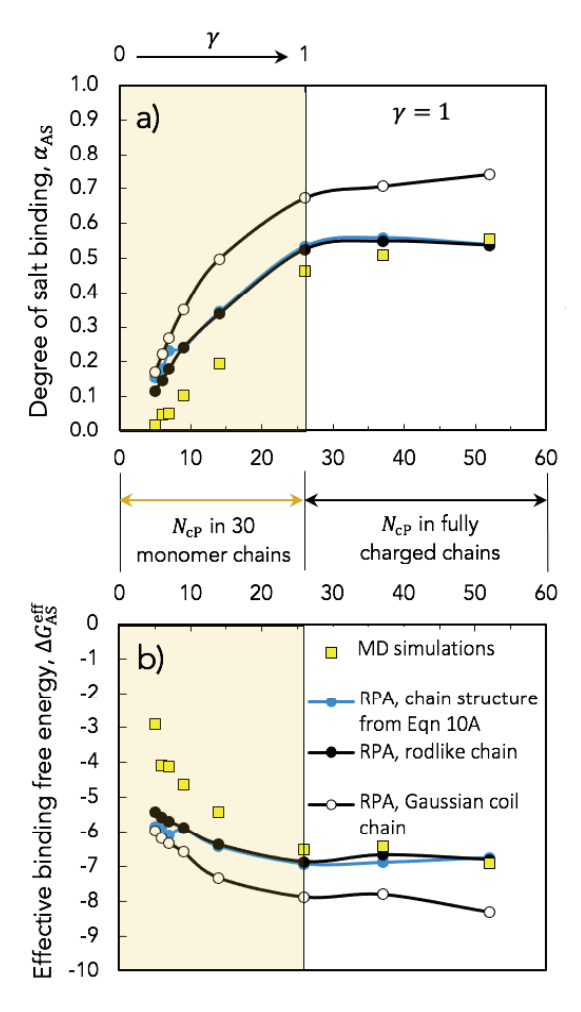


Figure S4. a) Binding fraction α_{AS} and b) effective binding free energy ΔG_{AS}^{eff} (in units of k_BT) for 30-monomer PAA chains with varying charge fraction (in the yellow-shaded region) and for fully charged PAA chains with varying chain length (in the white-shaded region) at $\omega_S=3$. The legend is the same as in Figure 5. Note that two monomers at each end of each chain are kept neutral and are not included in definitions of α_{AS} and γ .

At $\omega_S = 3$ (i.e., larger effective potassium size compared to $\omega_S = 1$), the dependence of α_{AS} and $\Delta G_{AS,2}^{eff}$ on the charge fraction γ at fixed chain length (in the yellow shaded area) and on the length of (fully charged) chains (in the white shaded area) closely resembles that for $\omega_S = 1$ in Figure 6: the rate of change of α_{AS} and $\Delta G_{AS,2}^{eff}$ with the charge fraction γ is much stronger than that with the length of "fully" charged chains. Also, similar to Figure 6, the agreement between the simulation results and the predictions improve as the chain

charge fraction increases. Note that, α_{AS} from the MD simulations obviously do not vary with the effective size of potassium, because α_{AS} is determined from ion-monomer RDFs.